Refereed Proceedings

The 12th International Conference on Fluidization - New Horizons in Fluidization Engineering

Engineering Conferences International *Year* 2007

Gas Fluidization and Pneumatic Conveying in Confined Beds: A Numerical Study

Yurong He* Thang Ngoc Cong†
Yulong Ding‡ Huilin Lu**

*University of Leeds, preyh@leeds.ac.uk
†University of Leeds, prentc@leeds.ac.uk
‡University of Leeds, y.ding@leeds.ac.uk
**Harbin Institute of Technology, Huilin@hit.edu.cn

GAS FLUIDIZATION AND PNEUMATIC CONVEYING IN CONFINED BEDS: A NUMERICAL STUDY

Yurong He[1], Thang Ngoc Cong[1], Yulong Ding[1*], Huilin Lu[2]
1, Institute of Particle Science and Engineering, University of Leeds, LS2 9JT, U.K.
2, Harbin Institute of Technology, Harbin, 154002, China
Tel.: +44 (0)113 343 2747; Fax: +44 (0)113 343 2405; E-mail: y.ding@leeds.ac.uk

ABSTRACT

Gas fluidization of fine particles in confined packed beds is numerically simulated by using the continuum-based two-fluid model. The body-fitted coordination is employed to treat the irregular geometry in the computational domain. Simulations are performed on both the bubbling regime in a partially packed bed and the pneumatic conveying regime in a fully packed bed. The modeling results are compared with experimental results by Donsi et al.(1) for the confined bubbling fluidization and confined conveying by Ding et al. (2) and reasonably good agreement has been achieved.

INTRODUCTION

Confined gas fluidisation refers to cases where interactions between fluidised particles and confining bodies are important in comparison with particle-particle and gas-particle interactions. Similarly confined pneumatic conveying refers to cases where interactions between conveyed solids particles and confining bodies are important. The confining bodies can be walls, inserts, and packing structures etc. (3, 4). Industrial examples of confined fluidisation and pneumatic conveying include blast furnaces for ironmaking where pulverised coal is injected into tuyeres for saving coke, filtration and waste heat recovery of flue gases, and circulating fluidised beds for power generation from coal, biomass and/or solids wastes. (5).

Ding et al. investigated experimentally the dilute pneumatic conveying of fine particles through packed beds. They found that the measured pressure drop of gas-solid two-phase mixtures flowing through packed beds agreed well with predictions by a modified version of the Ergun equation (6). Extensive work has also been done by the same group on the solids motion to study interactions between the suspended and packed particles (2). Suspended particles were found to distribute non-uniformly across the packed beds with particles spending more time in the wall region. Axial particle velocity was shown to change periodically with the radial position and the periodicity did not coincide exactly with the packed particle diameter (2). Despite of the considerable efforts, they are not systematic and expensive to execute. In some cases, the experimental observations are difficult to explain. As a consequence, numerical simulation work was initiated aiming at resolving these issues. The initial modeling shows that the predicted pressure drop and solids hold-up in the pneumatic regime agree well with the experimental results (7). This work is the

The 12th International Conference on Fluidization - New Horizons in Fluidization Engineering, Art. 86 [2007]

continuation of the effort to understand, by using the numerical technique, the detailed hydrodynamics of gas-solid two-phase flows in packed beds in both bubbling fluidization and pneumatic conveying regimes.
The continuum based two-fluid model is employed in this work with the irregular geometry treated with the body-fitted coordination. Both the partially and fully packed beds are considered, and the effects of the superficial gas velocity and the solids mass flux on the flow hydrodynamics are examined.

MODEL FORMULATION

The continuum based model uses the temporal and spatial averaging of particle and fluid variables along with the principles of mass, momentum and energy conservations. The details of the derivation of the equations are provided by Gidaspow (8) and He et al. (9).

Continuity and momentum equations

The accumulation of mass in each phase is balanced by the convective mass flows:

$$\frac{\partial}{\partial t}(\varepsilon_g \rho_g) + \frac{1}{J}\left[\frac{\partial}{\partial \xi}(\varepsilon_g \rho_g U_g) + \frac{\partial}{\partial \eta}(\varepsilon_g \rho_g V_g)\right] = 0 \tag{1}$$

$$\frac{\partial}{\partial t}(\varepsilon_s \rho_s) + \frac{1}{J}\left[\frac{\partial}{\partial \xi}(\varepsilon_s \rho_s U_s) + \frac{\partial}{\partial \eta}(\varepsilon_s \rho_s V_s)\right] = 0 \tag{2}$$

where ε_i is the concentration of phase i (i=s, g), ρ_i is the density of phase i, and subscripts g and s represent respectively the gas and particle phases, respectively. The transformed velocities of U_i and V_i, and Jacobian J are defined respectively as:

$$U = (u\xi_x + v\xi_y)J$$

$$V = (u\eta_x + v\eta_y)J$$

$$J = x_\xi y_\eta - x_\eta y_\xi \tag{3}$$

The momentum balance for the gas phase is given by the Navier-Stokes equation, modified to include an interphase momentum transfer term:

$$\frac{\partial}{\partial t}(\varepsilon_g \rho_g \varphi_g) + \frac{1}{J}\left[\frac{\partial}{\partial \xi}\varepsilon_g \rho_g U_g \varphi_g + \frac{\partial}{\partial \eta}\varepsilon_g \rho_g V_g \varphi_g\right] =$$

$$\frac{1}{J}\left\{\frac{\partial}{\partial \xi}\left[\frac{\mu_g}{J}\left(q_{11}\frac{\partial \varphi_g}{\partial \xi} + q_{12}\frac{\partial \varphi_g}{\partial \eta}\right)\right] + \frac{\partial}{\partial \eta}\left[\frac{\mu_g}{J}\left(q_{21}\frac{\partial \varphi_g}{\partial \xi} + q_{22}\frac{\partial \varphi_g}{\partial \eta}\right)\right]\right\} + S_g \tag{4}$$

where S_g is the source term of gas phase (9). The coordinate transformation are defined as:

$$q_{11} = (\xi_x^2 + \xi_y^2)J^2,\ q_{22} = (\eta_x^2 + \eta_y^2)J^2,\ q_{12} = q_{21} = (\xi_x \eta_x + \xi_y \eta_y)J^2 \tag{5}$$

The solids phase momentum balance in terms of transformed system is given by:

$$\frac{\partial}{\partial t}(\varepsilon_s \rho_s \varphi_s) + \frac{1}{J}\left[\frac{\partial}{\partial \xi}\varepsilon_s \rho_s U_s \varphi_s + \frac{\partial}{\partial \eta}\varepsilon_s \rho_s V_s \varphi_s\right] =$$

$$\frac{1}{J}\left\{\frac{\partial}{\partial \xi}\left[\frac{\mu_s}{J}\left(q_{11}\frac{\partial \varphi_s}{\partial \xi} + q_{12}\frac{\partial \varphi_s}{\partial \eta}\right)\right] + \frac{\partial}{\partial \eta}\left[\frac{\mu_s}{J}\left(q_{21}\frac{\partial \varphi_s}{\partial \xi} + q_{22}\frac{\partial \varphi_s}{\partial \eta}\right)\right]\right\} + S_s \tag{6}$$

where S_s is the source term of solid phase (9).

Kinetic-frictional stress model

Kinetic-frictional stress model is used in this work; see He et al. for details (9).

Interphase momentum exchange

In order to couple the momentum equations for the gas and particle phases, empirical models for the interphase force is used. For porosities less than 0.8, the pressure drop due to friction between the two phases can be described by the Ergun equation, whereas that for porosities higher than 0.8 can be described by the Wen-Yu equation. As a consequence, the interface momentum transfer coefficient, β_{gs}, is given by:

$$\beta_{gs} = \varphi\beta_{gs}\Big|_{\text{Ergun}} + (1-\varphi)\beta_{gs}\Big|_{\text{Wen \& Yu}} \tag{7}$$

$$\beta\Big|_{\text{Ergun}} = 150\frac{\varepsilon_s^2\mu_g}{\varepsilon_g^2 d^2} + 1.75\frac{\rho_g\varepsilon_s}{\varepsilon_g d}\left|\mathbf{U}_g - \mathbf{U}_s\right| \qquad \varepsilon_g \le 0.8 \tag{8}$$

$$\beta\Big|_{\text{Wen \& Yu}} = \frac{3C_d\varepsilon_g\varepsilon_s\rho_g\left|\mathbf{U}_g - \mathbf{U}_s\right|}{4d}\varepsilon_g^{-2.65} \qquad \varepsilon_g > 0.8 \tag{9}$$

$$\varphi = arctan\left(\frac{150\times 1.75(0.2-\varepsilon_s)}{\pi}\right) + 0.5 \tag{10}$$

$$C_d = \begin{cases} \dfrac{24}{\mathrm{Re}}\left(1+0.15\,\mathrm{Re}^{0.68}\right) & \mathrm{Re} \le 1000 \\ 0.44 & \mathrm{Re} > 1000 \end{cases} \tag{11}$$

where Re is the Reynolds number defined by $\mathrm{Re} = d\rho_g\left|\mathbf{U}_g - \mathbf{U}_s\right|/\mu_g$.

The dissipation of the fluctuating energy is expressed by (Gidaspow, 1994):

$$\gamma_s = 3(1-e^2)\varepsilon_s^2\rho_s g_o\theta\left[\frac{4}{d}\sqrt{\frac{\theta}{\pi}} - \frac{1}{J}\left(\frac{\partial U_s}{\partial\xi} + \frac{\partial V_s}{\partial\eta}\right)\right] \tag{12}$$

where e is the restitution coefficient of particles, d the particle diameter, and g_o the radial distribution function at contact. The radial distribution function, g_o, can be seen as a measure for the probability of interparticle contact. The equation of Bagnold (10) is used for g_o:

$$g_o = \left[1-\left(\frac{\varepsilon_s}{\varepsilon_{s,\max}}\right)^{1/3}\right]^{-1} \tag{13}$$

where $\varepsilon_{s,\max}$ is the maximum particle packing fraction.

Boundary conditions

Figure 1 shows the simulated bed partially packed with confining particles and the grids distribution. Assume the confined (large) particles are fixed in the bed in the whole simulation because the superficial gas velocity is not high enough to elutriate them. The body-fitted coordination is applied to make the grids fit the boundary of the packed coarse particles. Computation can be done on a rectangular transformed field with a square mesh. Since the domain has an unregulated boundary of conical base in the physical domain, it must be mapped onto a square computation domain.

For a two-dimensional coordinate system, the mapping functions $x(\xi,\eta)$ and $y(\xi,\eta)$ are obtained by solving the following equations:

$$q_{11}\frac{\partial^2 x}{\partial \xi^2} - 2q_{12}\frac{\partial^2 x}{\partial \xi \partial \eta} + q_{11}\frac{\partial^2 x}{\partial \eta^2} = -J^2[x_\xi P(\xi,\eta) + x_\eta Q(\xi,\eta)] \quad (14)$$

$$q_{11}\frac{\partial^2 y}{\partial \xi^2} - 2q_{12}\frac{\partial^2 y}{\partial \xi \partial \eta} + q_{11}\frac{\partial^2 y}{\partial \eta^2} = -J^2[(y_\xi P(\xi,\eta) + y_\eta Q(\xi,\eta)] \quad (15)$$

The grid control function $P(\xi,\eta)$ and $Q(\xi,\eta)$ is given as follows:

$$P(\xi,\eta) = -\sum_{i=1}^{n} a_i \,\mathrm{sgn}(\xi-\xi_i)\exp(-c_i|\xi-\xi_i|) - \sum_{j=1}^{m} b_j \,\mathrm{sgn}(\xi-\xi_j)\exp[-d_j\sqrt{(\xi-\xi_j)^2+(\eta-\eta_j)^2}] \quad (16)$$

$$Q(\xi,\eta) = -\sum_{i=1}^{n} a_i \,\mathrm{sgn}(\eta-\eta_i)\exp(-c_i|\eta-\eta_i|) - \sum_{j=1}^{m} b_j \,\mathrm{sgn}(\eta-\eta_j)\exp[-d_j\sqrt{(\xi-\xi_j)^2+(\eta-\eta_j)^2}] \quad (17)$$

The first summation term attracts ξ coordinates to the $\xi=\xi_i$ coordinate line in Eq. (16), and η coordinates to the $\eta=\eta_i$ coordinate line in Eq. (17). The second summation term attracts ξ and η coordinates toward the point (ξ_j,η_j). The coefficients a_i and b_j control the amplitude of attraction toward the corresponding lines and points, and the coefficients c_i and d_j determine the distance of influence from the line and points. The body-fitted coordinate grids used are shown in Figure 1.
At the inlet, all velocities are specified. The pressure is not specified at the inlet because of the incompressible gas phase assumption (relatively low pressure drop system). At the outlet, the pressure is specified (atmospheric). Initially, the velocities of both the gas and solid phases are set as the same as inlet velocity of the bed.
At the wall, the gas tangential and normal velocities are set to zero. The normal velocity of particles is also set to zero. The following boundary equations are applied for the tangential velocity and granular temperature at the wall:

$$v_{sw} = -\frac{6\mu_s\varepsilon_{s,max}}{\pi\rho_s\varepsilon_s g_o J\sqrt{3\theta(x_\xi^2+y_\xi^2)}}\left[(y_\xi^2+x_\xi^2)\frac{\partial v_s}{\partial \xi} - (y_\xi y_\eta + x_\xi x_\eta)\frac{\partial v_s}{\partial \eta}\right] \quad (18)$$

$$\theta_w = -\frac{k_s\theta}{e_w J\sqrt{(x_\xi^2+y_\xi^2)}}\left[(y_\xi^2+x_\xi^2)\frac{\partial \theta}{\partial \xi} - (y_\xi y_\eta + x_\xi x_\eta)\frac{\partial \theta}{\partial \eta}\right] + \frac{\sqrt{3}\pi\rho_s\varepsilon_s v_s g_o \theta^{3/2}}{6\varepsilon_{s,max} e_w} \quad (19)$$

where e_w is the restitution coefficient of the wall.

RESULTS AND DISCUSSION

Figure 2 shows the flow patterns in a confined fluidized bed packed to different extents at a superficial gas velocity of 2.0 m/s. Some large bubbles are seen to form in the bed without packing. The flow becomes more complicated and more small bubbles are formed with an increase in the extent of packing. In general, bubble number in the partially packing bed increases with increasing average bed voidage, whereas the bubble size decreases with increasing average bed voidage. Particles are found to move upward in the bed center and flow downward along the wall. Vortexes are formed in the downstream of the (large) packed particles. An increase in the extent of particle packing leads to more uniform distribution of the particle volume fraction.

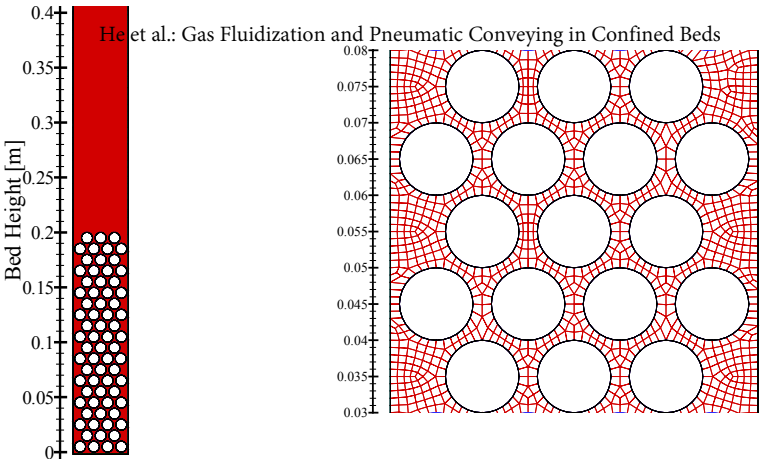

(a) Whole bed (b) Enlarged view

Figure 1. Grid distribution in confined fluidized bed.

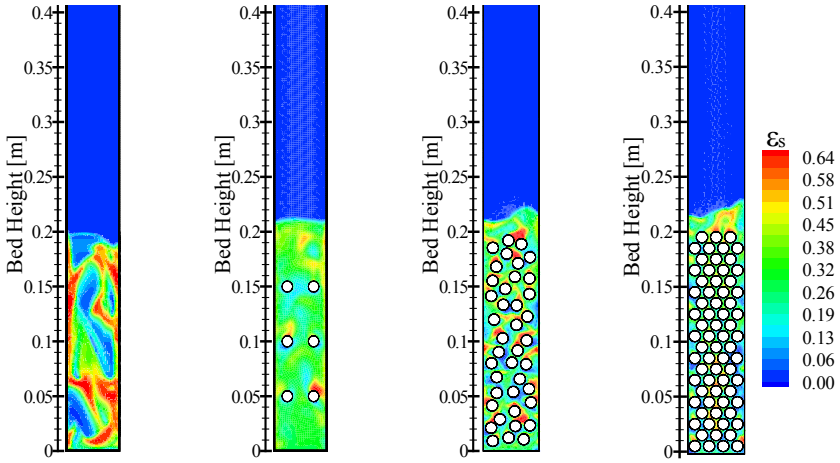

(a) ε =1.0 (b) ε =0.95288 (c) ε =0.68585 (d) ε =0.45024

Figure 2. Flow pattern in confined fluidized beds with various packed degrees (t=3.0s, u_g=0.2m/s).

Figure 3 illustrates the flow pattern at various superficial gas velocities in the confined bed partially packed to a packing fraction of ε =0.45024. The fine particle bed confined in the packed bed are seen to continuously with increasing superficial gas velocity and the dead zones in the downstream side decreases with increasing superficial gas velocity. The average volume fraction of the gas phase is plotted as a function of superficial gas velocities in Figure 4. One can see that the average volume fraction in the confined bed increases with increasing superficial gas velocities in a non-linear fashion. The data are found to fit well to Equation (20), which agrees well with the experimental results by Donsi etc. (1).

$$u = a\varepsilon^n \text{, n=5.93, a=0.815} \quad (20)$$

The 12th International Conference on Fluidization - New Horizons in Fluidization Engineering, Art. 86 [2007]

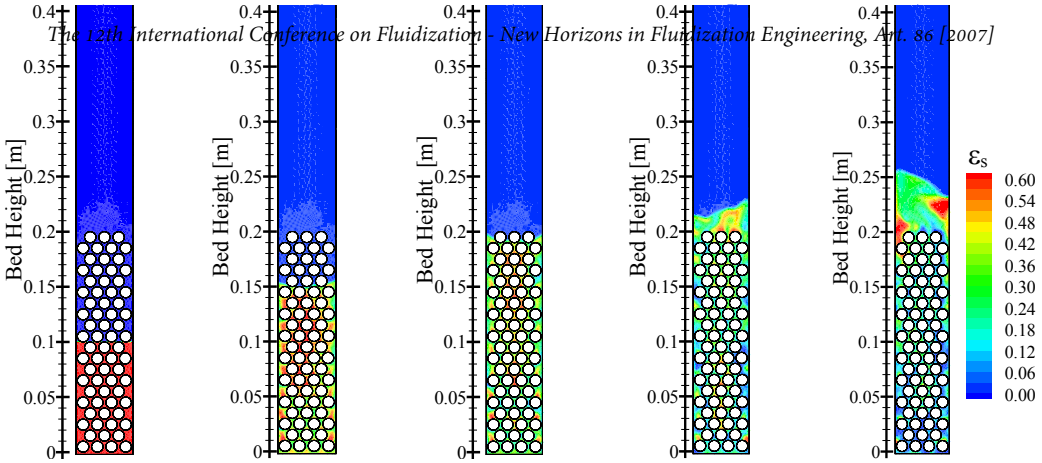

(a) Initial bed (b) u_g=0.05m/s (c) u_g=0.1m/s (d) u_g=0.2m/s (e) u_g=0.3m/s

Figure 3. Flow pattern in confined fluidized bed with various superficial gas velocities (t=3.0s).

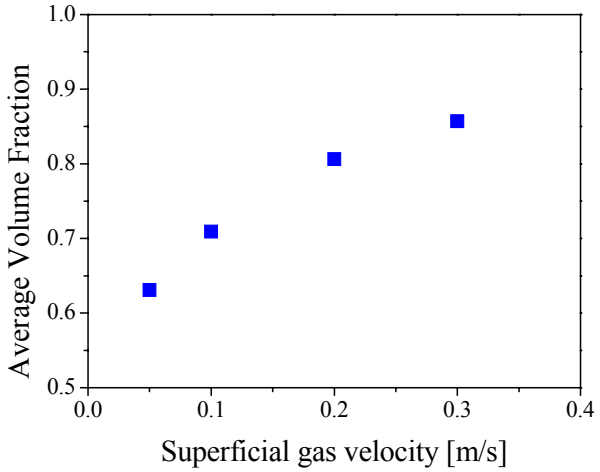

Figure 4. Average volume fraction distribution as functions of superficial gas velocities.

Figure 5 shows the flow pattern at various solids fluxes in the fully packed confining bed operated at a superficial gas velocity of 1.83 m/s. One can see that the greater the solids flux, the higher the solids volume fraction in the bed. This indicates that the solids hold-up is higher at a greater solids flux and the solids phase experiences greater resistance when flowing up through the packed bed. This agrees with the experimental observations of Ding et al. (2).

Figure 6 shows the pressure drop distribution as function of solids flux in the confined bed fully packed at a superficial gas velocity of 1.83 m/s. The pressure drop increases with increasing solids flux in almost a linear way. The pressure drop measured by Ding et al. is also shown in this figure. Qualitative agreement is seen between the modeling and experiments. More work is needed to elucidate the reasons for the difference.

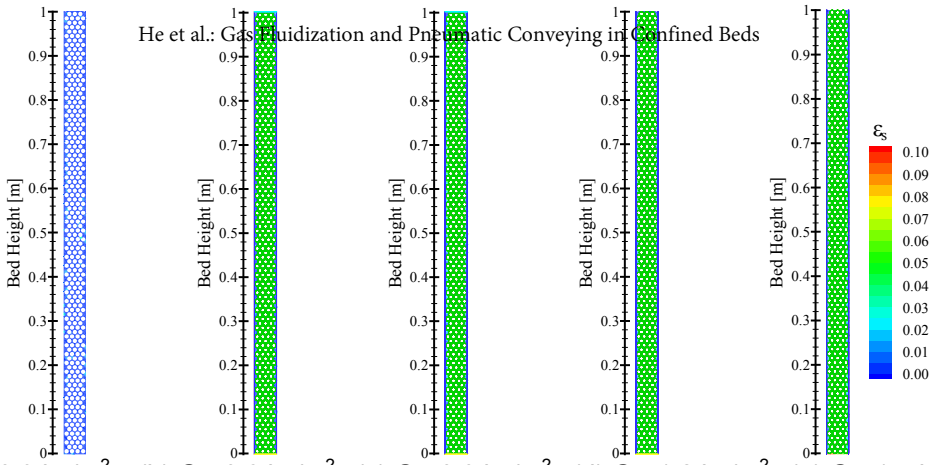

(a) G_s=0.3 kg/m^{2}s (b) G_s=0.6 kg/m^{2}s (c) G_s=0.9 kg/m^{2}s (d) G_s=1.2 kg/m^{2}s (e) G_s=1.5 kg/m^{2}s

Figure 5. Flow pattern in the confined fluidized bed operated with various solids flux (t=3.0s).

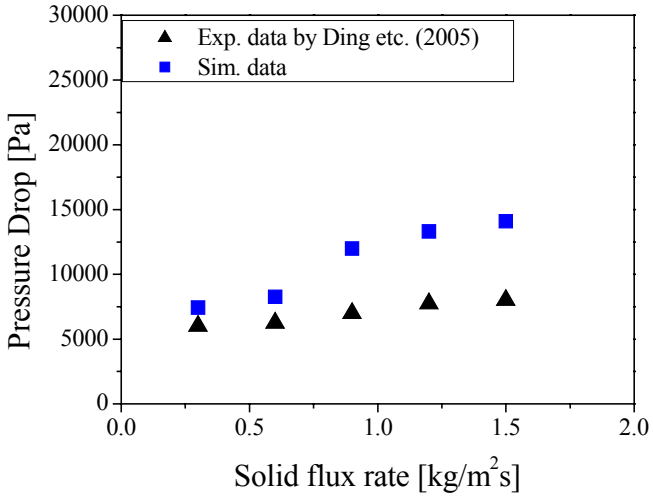

Figure 6. Pressure drop distribution as functions of solids flux.

CONCLUSIONS

Confined gas fluidization and pneumatic conveying of fine particles in in packed beds have been investigated numerically. The following conclusions have been obtained:

- Bubble number in a partially packed bed increases with increasing average bed voidage. Bubble size, on the other hand, decreases with increasing average bed voidage.
- Average volume fraction of the solids phase in partially packed beds depends on the superficial gas velocities in an exponential way, in consistent with experiments.
- Pressure drop depends on the solids flux in approximately linear way for fully packed beds.

ACKNOWLEDGMENT

This work was supported by Natural Science Foundation of China through Grant No. 20606006.

REFERENCES

[1] G. Donsi, G. Ferrari, B. Formisani, On the segregation mechanism of percolating fines in coarse-particle fluidized beds, Powder technology, 1988, 55: 153~158.
[2] Y.L. Ding, Z.L. Wang, D.S. Wen, M. Ghadiri, X.F. Fan and D.J. Parker, Solids behaviour in a gas–solid two-phase mixture flowing through a packed particle bed, Chemical Engineering Science, 2005b, 60: 5231~5239.
[3] L. Moldavsky, A. Goldshtein, K. Shuster, M. Fichman, D. Pnueli, M. Shapiro, C. Gutfinger, Confined fluidized bed—model and experiments, International Journal of Multiphase Flow, 2005, 31: 957~967.
[4] P. Vainshtein, M. Fichman, M. Shapiro, L. Moldavsky, C. Gutfinger, Fluidized bed in a confined volume, International Journal of Multiphase Flow, 1999, 25: 1431~1456.
[5] Y. B. Yang, et al, A diffusion model for particle mixing in a packed bed of burning solids, Fuel, 2005, 84(23): 213~225.
[6] Y.L. Ding, Z.L. Wang, D.S. Wen and M. Ghadiri, Hydrodynamics of gas–solid two-phase mixtures flowing upward through packed beds, Powder Technology, 2005a, 153: 13~22.
[7] Shuiqing Li, Yulong Ding, Dongsheng Wen, Yurong He, Modelling of the behaviour of gas-solid two-phase mixtures flowing through packed beds, Chemical Engineering Science, 2006, 61: 1922~1931.
[8] D. Gidaspow, Multiphase flow and fluidization: Continuum and kinetic theory descriptions, Academic Press Inc, 1994.
[9] He Yurong, Lu Huilin, Sun Qiaoqun, Yang Lidan, Zhao Yunhua, Dimitri Gidaspow, Hydrodynamics of gas-solid flow around immersed tubes in bubbling fluidized beds, Powder Technology, 2004, 145: 88~105.
[10] R. A. Bagnold, Experiments on a Gravity-Free Dispersion of Large Solid Spheres in a Newtonian Fluid Under Shear, Proc. R. Soc.. London, 1954, A225: 49~63.